The Journal of Infectious Diseases

SUPPLEMENT ARTICLE

Role of Transmembrane Protein 16F in the Incorporation of Phosphatidylserine Into Budding Ebola Virus Virions

Patrick Younan,[1,3,4] Mathieu Iampietro,[1,3,4] Rodrigo I. Santos,[1,3,4] Palaniappan Ramanathan,[1,3,4] Vsevolod L. Popov[1,4] and Alexander Bukreyev[1,2,3,4]

Departments of [1]Pathology and [2]Microbiology and Immunology and [3]Galveston National Laboratory, [4]University of Texas Medical Branch, Galveston

Viral apoptotic mimicry, which is defined by exposure of phosphatidylserine (PtdSer) into the outer leaflet of budding enveloped viruses, increases viral tropism, infectivity and promotes immune evasion. Here, we report that the calcium (Ca^{2+})–dependent scramblase, transmembrane protein 16F (TMEM16F), is responsible for the incorporation of PtdSer into virion membranes during Ebola virus infection. Infection of Huh7 cells with Ebola virus resulted in a pronounced increase in plasma membrane-associated PtdSer, which was demonstrated to be dependent on TMEM16F function. Analysis of virions using imaging flow cytometry revealed that short hairpin RNA-mediated down-regulation of TMEM16F function directly reduced virion-associated PtdSer. Taken together, these studies demonstrate that TMEM16F is a central cellular factor in the exposure of PtdSer in the outer leaflet of viral membranes.

Keywords. Ebola virus; TMEM16F; cellular scramblase; Viral Apoptotic Mimicry; Phosphatidylserine.

Ebola virus (EBOV) infection in West Africa during an outbreak extending late 2013 to early 2016 resulted in 28 616 probable and confirmed cases of EBOV disease, of which 11 310 fatalities were reported [1]. EBOV disease is associated with the rapid onset of nonspecific symptoms that result from multiple abnormalities including hypotension, leukopenia, thrombocytopenia, and disseminated intravascular coagulation [2, 3]. Furthermore, elevated levels of serum alanine and aspartate aminotransferases and D-dimers are detected. suggesting extensive liver damage and blood clot formation, respectively [4, 5]. Lymphopenia is pronounced in severe EBOV disease, and the extent of the release of inflammatory mediators known as the "cytokine storm" is inexorably linked to fatalities in EBOV-infected patients [6–13].

EBOV displays broad tissue tropism and has been shown to infect multiple cell types in the liver, spleen, adrenal glands, and other organs [14]. Antigen-presenting cells are targeted early during infection resulting in significant impairment of both the innate and adaptive immune responses [15]. Infection of monocytes and macrophages results in the release of proinflammatory mediators, which is probably a central contributor to the onset of a cytokine storm [16]. Unlike infection of these antigen-presenting cells, infection of dendritic cells results in their aberrant maturation, reduced cytokine production, and reduced specific stimulation of T cells, thus further blunting the initiation of an adaptive immune response [17–22].

As the most abundant anionic phospholipid of the plasma membrane, phosphatidylserine (PtdSer) is segregated within the inner leaflet during normal cellular conditions [23, 24]. During the later stages of apoptosis, cell stress, cellular activation or malignant transformation, the loss of PtdSer asymmetry is commonly observed [25–27]. Mechanistically, the altered PtdSer profile occurs because of the inhibition of cellular translocases, activation of PtdSer exporters, or increased activity of lipid-scrambling enzymes, such as scramblases. Significant evidence has demonstrated that virus-associated PtdSer increases viral infectivity and may broaden viral tropism while providing virion-associated immunosuppressive functions, which together have been termed "viral apoptotic mimicry" [28–35].

Asymmetric distribution of phospholipids in lipid bilayers is commonly observed in endosomal, Golgi, and plasma membrane but not in endoplasmic reticulum (ER)–associated bilayers [36, 37]. These findings provide evidence of potential viral egress pathways, which may enable budding virions with an opportunity to gain PtdSer-rich viral membranes. Flaviviruses, which include dengue virus, have been shown to bud into the lumen of the ER [38]; the luminal leaflet of the ER membrane is enriched for PtdSer, possibly indicating how dengue virus obtains its PtdSer-enriched viral membrane [39]. Several viruses including influenza virus, measles virus and human immunodeficiency virus (HIV) have been shown to bud from plasma membrane-associated regions termed lipid rafts, which in the context of viral infection are regulated specialized domains that permit association of cellular factors with viral proteins to facilitate assembly and budding, and which are also regions of concentrated PtdSer [40]. Similarly, EBOV has been shown to bud via elongation from the plasma membrane-associated lipid rafts rather than internal membranous organelles [41]. Recent evidence has suggested that the envelope of EBOV virions is enriched for PtdSer [29, 33].

Correspondence: A. Bukreyev, PhD, Department of Pathology and Department of Microbiology and Immunology, Galveston National Laboratory, Keiller Bldg, Room 3.145, University of Texas Medical Branch, 301 University Blvd, Galveston, TX 77555-0609 (alexander.bukreyev@utmb.edu).

The Journal of Infectious Diseases® 2018;218(S5):S335–45

DOI: 10.1093/infdis/jiy485

Specific cellular factors involved in trafficking PtdSer between the inner and outer leaflet have been identified, which appear to be active during specific cellular processes. For instance, XK-related protein 8 (XKr8) is a plasma membrane-associated scramblase, which is cleaved during apoptosis by active caspases 3 and 7 [42]. Hence, detection of apoptotic cells using annexin V probes is dependent on XKr8 phospholipid scrambling activity. A recent publication indicated that XKr8 may play a role in PtdSer incorporation into budding virions [43]. Transmembrane protein 16F (TMEM16F), also known as ANO6, is a calcium-dependent scramblase associated with PtdSer translocation during periods of cellular stress [44]. Because TMEM16F has been shown to colocalize with lipid rafts, and EBOV virions are likely to obtain PtdSer-enriched membranes through budding via lipid rafts, we investigated whether TMEM16F or the recently identified factor, XKr8, may influence the relative abundance of PtdSer associated with viral membranes.

METHODS

Experiments Under Biosafety Level 4 Containment

All work with EBOV was performed within the Galveston National Laboratory biosafety level 4 (BSL-4) laboratories. Flow cytometry samples were fixed with 4% buffered paraformaldehyde in phosphate-buffered saline (PBS) for 48 hours according to the University of Texas Medical Branch–approved standard operating procedure protocol, removed from the BSL-4 laboratories, and analyzed at the University of Texas Medical Branch's Flow Cytometry Core Facility. Samples for Western blot analysis were prepared by lysis of cells with 4× sodium dodecyl sulfate Laemmli buffer, followed by incubation at 95°C for 15 minutes, vortexing, and removal from BSL-4 laboratories. Cells for confocal microscopy were placed on slides, stained, fixed by incubation in 4% paraformaldehyde for 72 hours and removed from the BSL-4 laboratories. Staining and mounting procedures are described below.

Viruses

Recombinant EBOV, strain Mayinga, expressing green fluorescent protein (GFP) and wild-type EBOV were recovered from complementary DNA, as described elsewhere [45, 46], and propagated by 3 passages in Vero E6 cell monolayers. Viral stocks were quantified by plaque titration in Vero E6 monolayers, as described elsewhere [47].

Parental and Short Hairpin RNA Cell Lines

Huh7 and Vero E6 cell lines were obtained from the American Type Culture Collection and cultured in Dulbecco modified Eagle medium and modified Eagle medium, respectively, supplemented with 10% heat-inactivated fetal bovine serum (Thermo Fisher Scientific), 1% HEPES (Corning), 1% nonessential amino acids (Sigma-Aldrich), 1% sodium pyruvate (Sigma-Aldrich), and 2% PenStrep mix (Thermo Fisher Scientific). Lentiviral vectors targeting TMEM16F and XKr8 (both from Santa Cruz Biotechnology) and scrambled short hairpin RNAs (shRNAs) (Thermo Fisher Scientific) were used to transduce Huh7 cells in 6-well plates. After 48 hours, cells were selected with puromycin at a concentration of 5 μg/mL. The relative knockdown was determined by Western blotting and decreased functional analysis, as described in Supplementary Figure 1.

Confocal Microscopy

Huh7 cells (10 000 cells per well) were cultured in a 24-well plate on positively charged coverslips (Thermo Fisher Scientific) incubated overnight at 37°C. Cells were infected with EBOV at the indicated multiplicity of infection (MOI) the next morning and cultured for an additional 48 hours. Cells were washed twice with PBS and stained with 200 ML of staining buffer (1× annexin V binding buffer) containing antibodies and annexin V conjugates. Rabbit immune serum against EBOV viruslike particles (VLPs) (Integrated BioTherapeutics) were diluted at 1:100 in stain buffer and used to stain for glycoprotein (GP). PtdSer was detected using annexin V–Alexa 647 conjugate (Thermo Fisher Scientific). After 30-minute incubation at room temperature, slides were washed 3 times in stain buffer, incubated with the secondary antibody: donkey anti-rabbit conjugated with Alexa Fluor 488 (Thermo Fisher Scientific) and/or anti-mouse Alexa 647 (Thermo Fisher Scientific), diluted at 1:200 in stain buffer for 30 minutes, and washed as described above. Next, cells were incubated with 6- diamidino-2-phenylindole-dihydrochloride (Thermo Fisher Scientific) at 1 μg/mL for 2 minutes and washed 3 times in PBS. Slides were then fixed in paraformaldehyde 4% and removed from BSL-4 laboratories, as described above. Coverslips were mounted onto microscope slides using PermaFluor mounting medium (Thermo Fisher Scientific) and analyzed using an Olympus FV1000 confocal microscope. All images were acquired using a ×60 oil objective. Image analysis was performed using Olympus FluoView viewer software (version 4.2).

Flow Cytometry Analysis

EBOV-infected or mock infected Huh7 cells were harvested, centrifuged, and stained in 1× annexin V binding buffer with anti-VLP serum (1:100) and annexin V–Alexa Fluor 647 (1:200). Cells were washed twice in 1× annexin V buffer and stained with an anti-rabbit Alexa Fluor 488–labeled secondary antibody. After staining, cells were washed 3 times with 1× annexin V staining buffer and fixed in 10% formalin (Thermo Fisher Scientific). EBOV-GFP was used in parallel to experiments performed using wild-type EBOV, which enabled detection of the relative percentages of infected cells at the indicated time points. Flow cytometry was performed using a FACS Fortessa (BD Biosciences) instrument.

Imaging Flow Cytometry Analysis

Cells were infected, harvested, and stained as described for flow cytometry experiments above. Hoescht staining was performed to visualize nuclei after fixation of cells (Thermo Fisher

Scientific). A minimum of 2000 events/images were used for cellular analysis purposes. Analysis of virion-associated PtdSer was performed after overnight polymer-based (Alstem) precipitation of virions isolated from cell-free supernatants of the cell lines indicated in the text. Virions were pelleted at 2000 rpm at 4°C for 30 minutes and were resuspended in 100 ML of 1× annexin V staining solution containing anti-VLP serum and annexin V–phycoerythrin. Labeled virions were then fixed in 10% formalin and analyzed using an AMNIS Flowsight Imaging flow cytometer (EMD Millipore). The purity of the virions was monitored and confirmed during imaging flow cytometry experiments with gating by "aspect ratio" on the y-axis and "area" on the x-axis in the bright-field channel, using IDEAS version 2.0 software.

Western Blotting

Precast gradient Sodium dodecyl sulfate–polyacrylamide gel electrophoresis gels were purchased from Thermo Fisher Scientific. Cell lysates were prepared in 4× Lamenli buffer (Thermo Fisher Scientific), as required before removal from BSL-4 facilities. Samples were diluted to 1× in RIPA buffer before being boiled and loaded onto gels. Separated proteins were blotted onto nitrocellulose membranes using the I-Blot2 system (Thermo Fisher Scientific). Anti-VLP serum, anti-GP anti-VP40m and anti–nucleoprotein (NP) antibodies were purchased from Integrated BioTherapeutics. Glyceraldehyde 3-phosphate dehydrogenase antibody was purchased from Thermo Fisher Scientific. Anti-ANO6 (TMEM16F) antibody was purchased from Sigma-Aldrich, anti-XKr8 antibody from Invitrogen, and secondary antibodies from Santa Cruz Biotechnology. Blocking and staining was performed with BLOTTO Blocking Buffer (5% milk in PBS-Tween).

Drug Inhibitors

R5421 was purchased from Endotherm, A23187 from Sigma-Aldrich, and 1,2-bis(*o*-aminophenoxy)ethane-*N*,*N*,*N*′,*N*′-tetraacetic acid (BAPTA) from Thermo Fisher Scientific. All drugs were initially dissolved in dimethyl sufoxide and used at the concentrations indicated in the figures.

Statistical Analysis

Each experiment was performed in triplicate to rule out experimental bias or random error. Data were analyzed using statistical methods described in figure legends using GraphPad Prism 6 software. Differences were considered statistically significant at $P < .05$. Mean and standard errors of the mean were calculated for all graphs.

RESULTS

PtdSer Exposure During EBOV Infection: Dependence on TMEM16F

Our initial studies investigated whether EBOV infection itself could increase the relative levels of plasma membrane-associated PtdSer. As shown in Figure 1A, EBOV infection had a profound effect on plasma membrane-associated PtdSer levels, as determined by confocal microscopy. Virtually no significant annexin V staining was observed in mock-infected, Huh7/shScramble control cells; however, the outer leaflet of the plasma membrane of EBOV-infected cells was clearly delineated by annexin V staining. A near-uniform increase in annexin V staining was observed specifically in cells positive for the EBOV sole envelope GP (GP^+ cells), whereas annexin V staining on uninfected cells (GP^-) was nearly completely absent.

To determine the role of the previously described cellular scramblases on virus-induced cell surface translocation of PtdSer, Huh7-based cell lines expressing shRNAs for XKr8, TMEM16F, and scrambled shRNAs were selected and expanded after culture in the presence of puromycin. The relative decrease in expression levels and known functional activities (eg, calcium ionophore induction of PtdSer flippling) was determined before experimentation with EBOV to demonstrate consistency of our cell lines with findings published elsewhere (Supplementary Figure 1*A* and 1*B*). Unlike the control scrambled shRNA cell line, knockdown expression of TMEM16F resulted in the near-complete absence of detectable cell surface-associated PtdSer in EBOV-infected cells (Figure 1B). The relative level of annexin V staining on GP^+ Huh7/shXKr8 cells (Supplementary Figure 1*C*) was equivalent to that observed in GP^+ Huh7/shScramble cells (Figure 1A).

These results were further confirmed by analysis of cells with imaging flow cytometry using an AMNIS system, which combines flow analysis with fluorescent microscopy. Representative images of mock-infected and EBOV-infected Huh7/shScramble and EBOV-infected Huh7/shTMEM16F are shown in Figure 1C. Examination of the GP expression profile in EBOV-infected Huh7/shScramble and EBOV-infected Huh7/shTMEM16F cells demonstrated that decreased expression of TMEM16F resulted in a minor reduction in GP when cells were infected at an MOI of 1 plaque-forming unit/cell for 48 hours (Figure 1D); however, the relative translocation of PtdSer to the outer leaflet of the plasma membrane was significantly reduced in the TMEM16F shRNA cell line (Figure 1D). Taken together, these findings indicate that TMEM16F expression is responsible for the EBOV-induced translocation of PtdSer to the outer leaflet of infected cells.

EBOV Infectivity Reduced by Disabling of TMEM16F

As EBOV virion-associated PtdSer has been shown to increase viral infectivity, we investigated the ability of EBOV derived from Huh7/shScramble and the Huh7/shTMEM16F cell lines to spread between cells. To observe spread of infection to uninfected cells, EBOV propagated in wild-type Vero E6 cells was added at a low MOI of 0.3 plaque-forming unit/cell, and cells were incubated for 48 hours. As shown by confocal microscopy in Figure 2A, a clear reduction in spreading infection was observed in Huh7 cells, in which TMEM16F expression was knocked down by shRNAs. Using a recombinant infectious

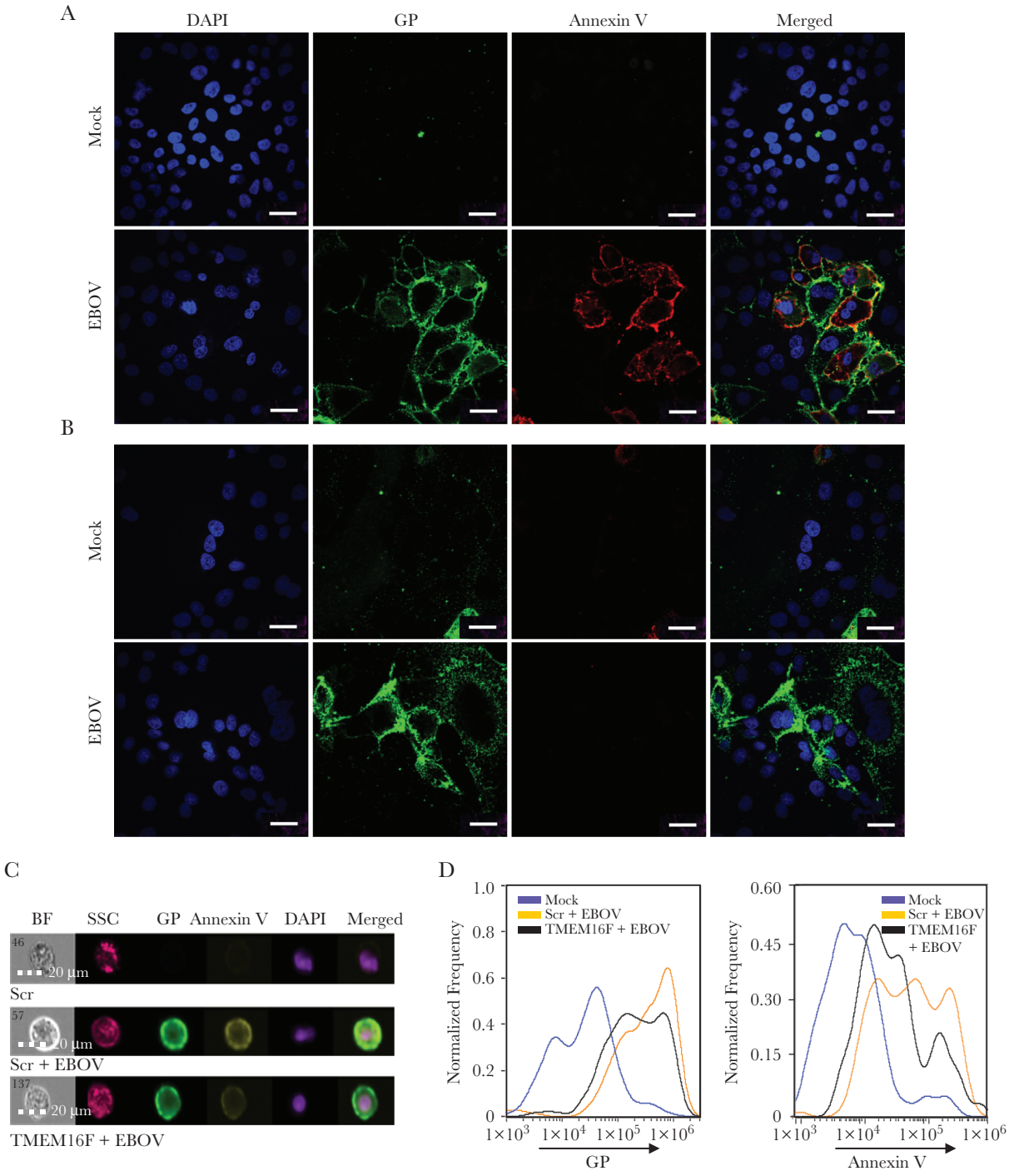

Figure 1. Ebola virus (EBOV)–induced extracellular expression of phosphatidylserine (PtdSer) is dependent on transmembrane protein 16F (TMEM16F) function. Huh7 cells were transduced with lentiviral vectors encoding scrambled short hairpin RNA (shRNA) (Scr) or shRNAs specific for TMEM16F and infected with EBOV at a multiplicity of infection of 1 plaque-forming unit/cell. *A, B,* Translocation of PtdSer to the outer leaflet of the plasma membrane in EBOV-infected Huh7/shScramble (*A*) or Huh7/shTMEM16F (*B*) cells. Targeted knockdown of TMEM16F results in decreased levels of plasma membrane-associated PtdSer (scale bar represents 30 µm). *C–E,* Imaging flow cytometry analysis of mock-infected and EBOV-infected shRNA cell lines. *C,* Representative images of mock-infected and EBOV-infected Huh7/shScramble and Huh7/shTMEM16F cell lines. The merged image is based on glycoprotein (GP), annexin V, and 4′,6-diamidino-2-phenylindole (DAPI). *D,* Relative levels of EBOV GP (*left*) and annexin V staining (*right*) of mock-infected and EBOV-infected Huh7/shScramble and Huh7/shTMEM16F cell lines. See Supplementary Figure 2*B* for gating strategy. Panels *A* and *B* are representative of 1 of 7 and panels *C* and *D* are representative of 1 of 3 independent experiments. Abbreviations: BF, bright field; SSC, side scatter.

EBOV expressing GFP from an added gene (EBOV-GFP) [45], we determined the relative infectivity rate of virus propagated in the Huh7/shScramble and Huh7/shTMEM16F cell lines. Compared with the Huh7/shScramble control cell line, the percentage of GFP$^+$ cells was significantly reduced 48 hours after infection in the Huh7/shTMEM16F cell line (Figure 2B). Of

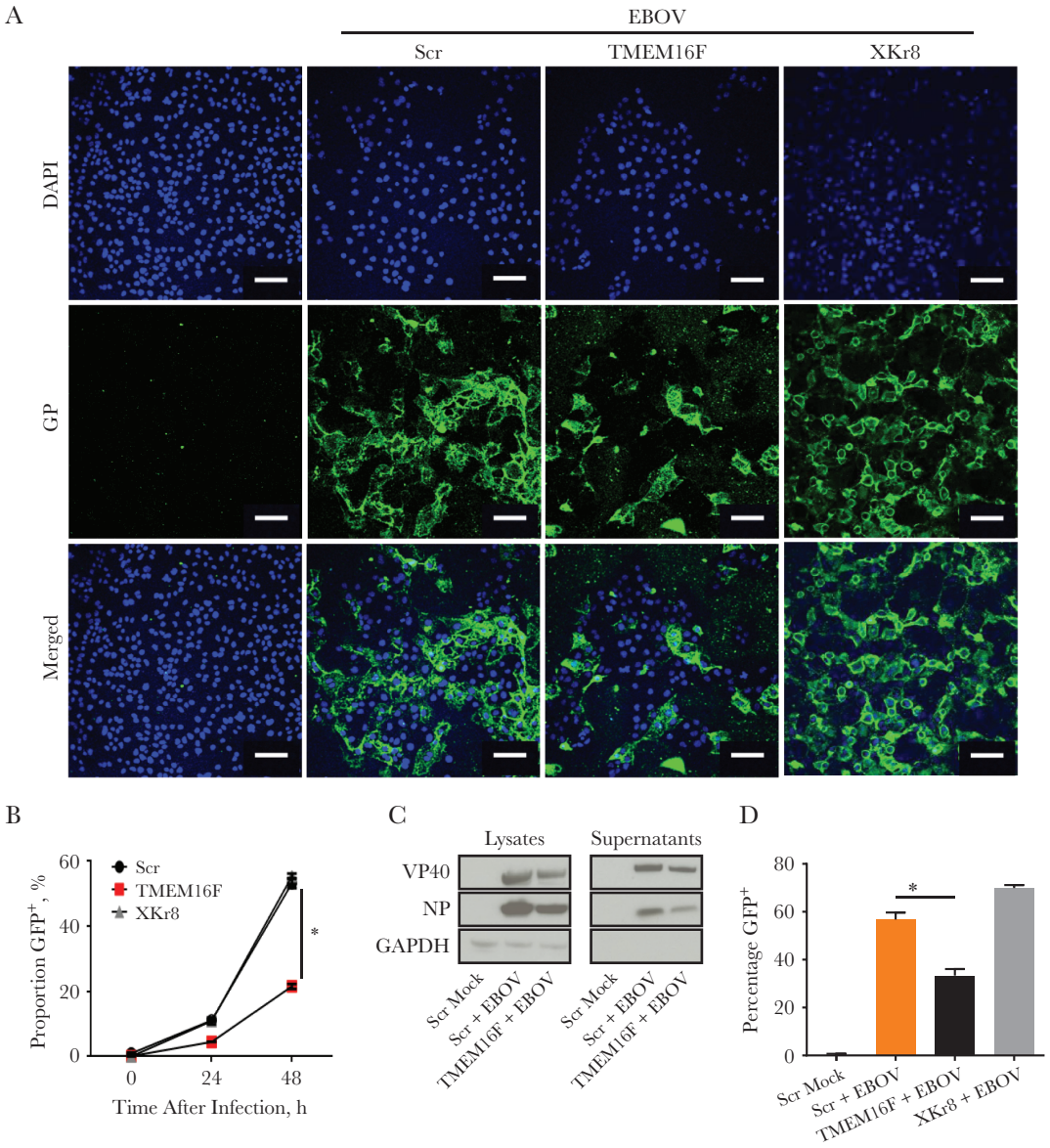

Figure 2. Blocking transmembrane protein 16F (TMEM16F) function reduces the levels of viral membrane-associated PtdSer leading to decreased infectivity. *A,* Huh7/short hairpin (sh)Scramble, Huh7/shTMEM16F and XK-related protein 8 (XKr8) cell lines were mock infected or infected with Ebola virus (EBOV) at a multiplicity of infection (of 0.3 plaque-forming unit /cell for 48 hours. Cells were stained for EBOV glycoprotein (GP) to determine the relative number of infected cells. (Scale bar represents 40 μm). *B,* Cells were infected with EBOV expressing green fluorescent protein (GFP) and analyzed by flow cytometry to determine the relative percentages of infected (GFP^+) cells at 24 and 48 hours. *C,* Amount of viral proteins in lysates and supernatants determined at 48 hours in Huh7/shScramble or Huh7/shTMEM16F shRNA cell lines. *D,* Supernatants from Huh7/shScramble and Huh7/ shTMEM16F cells were added to Vero E6 cells for 20 hours to determine the relative production of infectious virus. Means shown in graphs are from triplicate samples, with standard deviations and are representative of 3 independent experiments, $^*P < .001$ (Student *t* test). Abbreviations: DAPI, 4′,6-diamidino-2-phenylindole; Scr, scrambled shRNA.

Huh7/shScramble cells, 58% were infected (GFP^+), compared with only 21% of Huh7/shTMEM16F cells. The level of annexin V expression on Huh7/shXKr8 cell line was similar to that observed in Huh7/shScramble cells (Supplementary Figure 2*A* and 2*B*). The observation was further supported by flow cytometry findings (Supplementary Figure 1D).

Analysis of cell lysates and supernatants revealed that both intracellular and extracellular viral content were significantly reduced in samples collected from the Huh7.TMEM16F shRNA cell line, compared with those obtained from Huh7/shScramble cells (Figure 2C). As the spread of viral infection was significantly reduced, the reduction in viral protein content is most likely a reflection of the decreased rate of infection and not due to a direct reduction in viral replication within infected cells. Consistent with the decrease in viral proteins in supernatants, equal volume infection of Vero E6 cells with cell-free supernatants revealed a significantly reduced viral titer in supernatants harvested from EBOV-infected Huh7.TMEM16F cells (Figure 2D).

Although reduced PtdSer translocation to the plasma membrane during EBOV infection was observed in the TMEM16F. shRNA cell line (Figure 1B), it is feasible that viral membrane-associated PtdSer may remain unabated in EBOV particles during viral egress. Hence, to determine whether the observed decrease in infectivity coincided with reduced virion-associated PtdSer, we examined the relative incorporation of PtdSer into the outer leaflet of the viral membrane, using an imaging flow cytometry assay developed with EBOV VLPs (Supplementary Figure 3). Although the magnification of the AMNIS system is well below that required to visualize individual viral particles, we took an approach similar to that used to analyze features of exosomes [48], which are smaller than EBOV virions (30–120 vs 80 nm × 1000 nm, respectively) [49]. Huh7/shScramble and Huh7/shTMEM16F cell lines were infected with EBOV at an MOI of 0.3 plaque-forming unit/cell and cultured for 72 hours. Virions in cell-free supernatants were precipitated and resuspended in annexin V staining buffer, stained for GP and annexin V, fixed, and analyzed by imaging flow cytometry.

As shown in Figure 3A, individual particles were readily detectable by bright-field analysis, and a 4–5-fold decrease in the relative ratio of annexin V to GP was clearly visible in virions purified from Huh7/shTMEM16F compared with Huh7/shScramble cells. The GP^+ population was then gated (Figure 3B) and subsequently analyzed for the relative levels of PtdSer incorporation into viral membrane using annexin V staining (Figure 3C). A clear reduction in virion-associated PtdSer was observed in virions derived from Huh7/shTMEM16F cells compared with virus isolated from Huh7/shScramble cells. These findings parallel the results from Figure 1, which demonstrated a decrease in cell surface staining of annexin V in Huh7/shTMEM16F cells and suggest that PtdSer incorporation into virions is the result of increased plasma membrane–associated PtdSer.

Blocking Ca^{2+}-Dependent Signaling and Pharmacological Inhibition of TMEM16F Reduces PtdSer Translocation During EBOV Infection

TMEM16F function is dependent on an increase in cytosolic Ca^{2+} levels [44]; hence, blocking or reducing intracellular calcium levels was expected to reduce PtdSer translocation during EBOV infection. Using the cell-permeable calcium chelator, BAPTA AM, to reduce cytosolic Ca^{2+} levels, we observed a significant decrease in plasma membrane-associated PtdSer after EBOV infection, compared with untreated, EBOV-infected Huh7 cells, by both confocal microscopy and flow cytometry (Figure 4A–4C).

Although the decrease in annexin V expression in BAPTA AM–treated cells suggests that the translocation of PtdSer observed during EBOV infection is calcium dependent, it does not specifically verify the role of TMEM16F as observed by shRNA knockdown in Figure 1. Therefore, a previously described inhibitor of TMEM16F, R5421 [50], was used to further verify the specific role of TMEM16F in the observed EBOV-induced translocation of PtdSer. Huh7 cells were treated with various concentrations of R5421, incubated for 48 hours, stained with annexin V, and analyzed by flow cytometry. A clear dose-dependent decrease in annexin V staining was observed when Huh7 cells were infected with EBOV at increasing concentrations of R5421 (Figure 5A). Consistent with a decrease in annexin V staining resulting in decreased viral infectivity, the overall percentage of EBOV-infected, GFP^+ Huh7 cells also decreased in a dose-dependent manner (Figure 5B). Similarly, infection of Vero E6 cells with cell-free supernatants collected from Huh7 cells treated with R5421 exhibited a significant reduction in viral titers (Figure 5C). These results further demonstrate that role of TMEM16F in EBOV-induced exposure of membrane-associated PtdSer and demonstrate its importance in promoting viral infectivity.

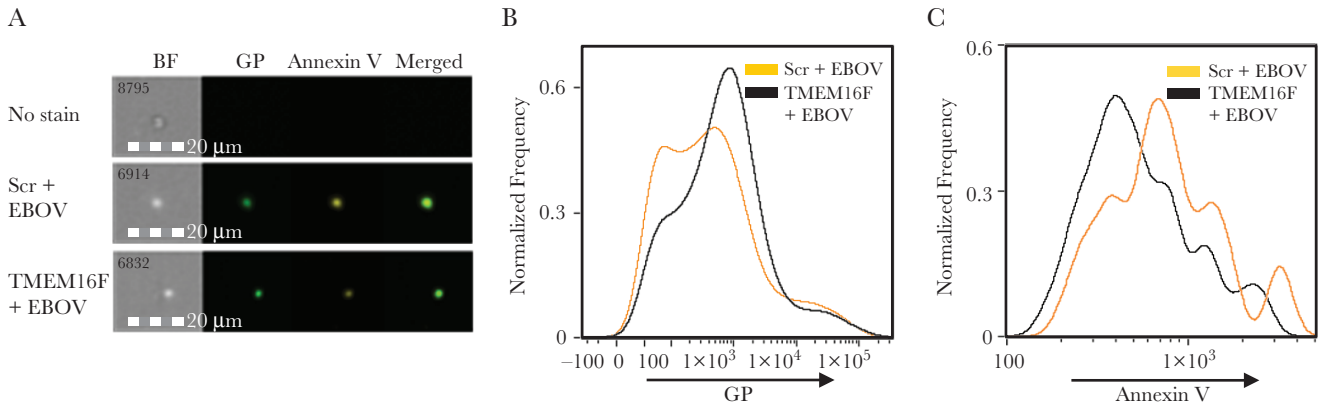

Figure 3. Blocking transmembrane protein 16F (TMEM16F) function reduces the levels of viral membrane-associated PtdSer, leading to decreased infectivity. *A,* Representative images from imaging flow cytometry analysis of virions purified from Huh7/short hairpin (sh)Scramble and Huh7/shTMEM16F Ebola virus (EBOV)–infected cells. The merged image is based on GP and annexin V. *B,* Relative glycoprotein (GP) expression profiles. *C,* Relative annexin V incorporation in GP^+ population. Abbreviations: BF, bright field; Scr, scrambled shRNA.

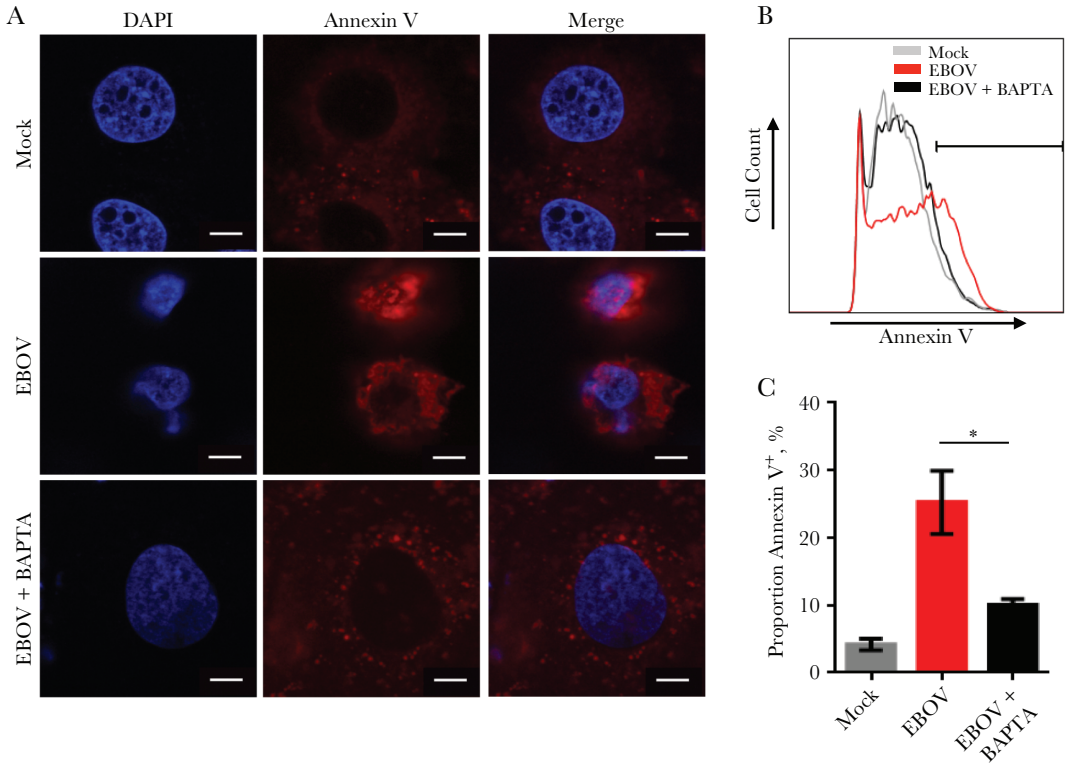

Figure 4. Blocking calcium (Ca^{2+})–dependent signaling reduces annexin V exposure during Ebola virus (EBOV) infection. The addition of calcium chelator (BAPTA) was used to block calcium-dependent translocation of PtdSer; findings shown represent 1 of 2 independent experiments. *A,* The extent of PtdSer translocation analyzed by confocal microscopy (scale bar represents 10 μm). *B,* Histograms depicting relative annexin V levels analyzed by flow cytometry. Gate shown was used to compare expression levels. *C,* Graphic representation of the percentage of annexin V^+ cells from flow cytometry samples in panel B. Mean values are shown for triplicate samples, with standard deviations. $^*P < .01$ (Student *t* test). Abbreviation: DAPI, 4′,6-diamidino-2-phenylindole.

To determine whether PtdSer translocation is dependent on expression of a specific viral protein, Huh7 cells were transfected with plasmids encoding individual viral proteins including nucleoprotein (NP), GP, or the major matrix protein located under the viral membrane, VP40, incubated for 48 hours, stained with annexin V, and analyzed by flow cytometry. As observed in Figure 6, transfection with GP or VP40, but not NP, resulted in significant increase in plasma membrane–associated PtdSer

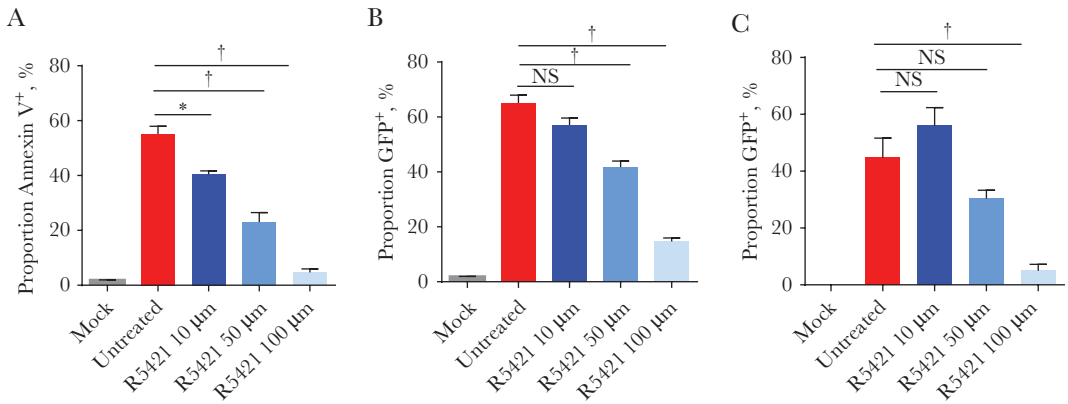

Figure 5. Blocking transmembrane protein 16F (TMEM16F) function with R5421 reduces viral infectivity. *A,* Huh7 cells were treated with an increasing concentration of R5421 to determine whether blocking TMEM16F reduces plasma membrane-associated phosphatidylserine after Ebola virus (EBOV) infection. Cells were incubated for 48 hours, stained with annexin V and analyzed by flow cytometry. *B,* Percentages of cells expressing green fluorescent protein (GFP) at 48 hours after EBOV infection of mock-infected or R5421-treated Huh7 cells. *C,* Viral production from R5421-treated Huh7 cells was determined by adding cell-free supernatants to Vero E6 cells. At 20 hours after infection, cells were fixed and analyzed for GFP expression by flow cytometry. Means shown in graphs are from triplicate samples, with standard deviations; results are representative of 3 independent experiments. $^*P < .01$; †$P < .001$. Abbreviation: NS, not significant (Student *t* test).

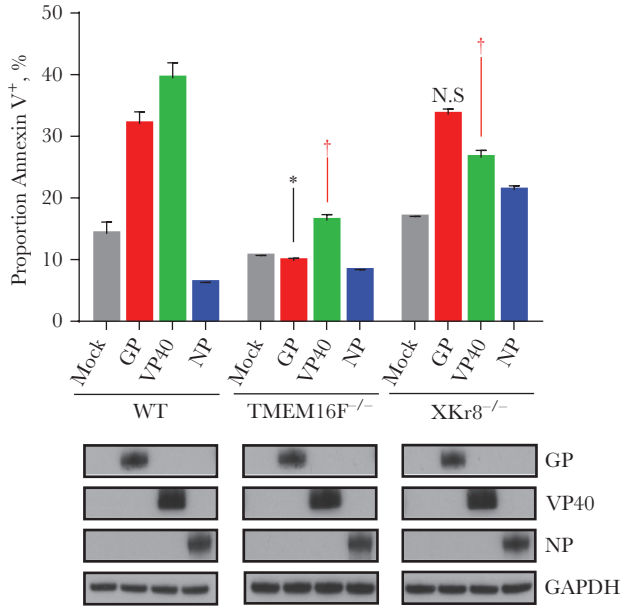

Figure 6. Viral protein dependent translocation of annexin V. Relative annexin V staining induced by transfection of Huh7 cell lines with plasmids encoding individual viral proteins determined by flow cytometry 48 hours after transfection. Western blot analyses were performed to verify expression of viral proteins glycoprotein (GP), VP40 and nucleoprotein (NP) (*lower panel*). Means and standard deviations are shown for triplicate samples from 1 of 2 independent experiments. $^{*}P < .001$ (knockdown cell line vs mock-infected cells); †$P < .001$ (viral protein expression compared with corresponding mock-infected sample for a given cell line); NS, not significant (Student *t* test). Abbreviations: GAPDH, glyceraldehyde 3-phosphate dehydrogenase; TMEM16F, transmembrane protein 16F; WT, wild type; XKr8, XK-related protein 8.

in Huh7/shScramble cells. A notable decrease was observed by flow cytometry in Huh7/shTMEM16F cell line transfected with GP or VP40, whereas minor to no significant changes were observed in the Huh7/shXKr8 cell line. Taken together, these results confirm the role of TMEM16F in EBOV-induced translocation of PtdSer to surface of infected cells and demonstrate that viral GP and VP40 antigens trigger the translocation of PtdSer to the outer leaflet of the plasma membrane.

DISCUSSION

To date, the mechanism by which enveloped viruses that bud from the plasma membrane obtain viral membranes enriched with PtdSer in their outer leaflet remains largely unknown [51]. In the current study, we investigated the mechanism by which budding EBOV virions obtain viral membranes enriched with PtdSer in the outer leaflet. We have shown that infection of Huh7 cells results in a pronounced increase in extracellular PtdSer and, as shown in Figures 1 and 2, the Ca^{2+}-dependent scramblase, TMEM16F, is primarily responsible for this occurrence (a proposed model is shown in Figure 7).

Although minimal effects of the membrane-associated scramblase XKr8 were observed in these studies, a recent publication by Nanbo et al [43] demonstrated that XKr8 may contribute to the incorporation of PtdSer into budding virions. We cannot rule out the possibility that, in conditions of prolonged culture or in other cell types, this scramblase may play a role in PtdSer incorporation into virions. It is possible that use of the surrogate nonpathogenic system, representing VLPs, which include only 3 (GP, VP40, NP) of 7 EBOV proteins in the study by Nanbo et al [43], contributed to the differences observed in these studies.

As we compared the roles of both TMEM16F and XKr8 in head-to-head experiments, our results clearly indicated that TMEM16F plays a more prevalent role in our experimental model. As indicated in Figure 1 and Supplementary Figures 1*C* and 2, shRNAs targeting XKr8 did not result in a significant reduction of membrane-associated PtdSer in EBOV-infected cells, whereas in TMEM16F knockdown cells PtdSer was almost undetectable. In addition, the infectivity of virus propagated in XKr8 cells was not significantly reduced compared with virus harvested from the TMEM16F shRNA cell line (Figure 2B and 2D). Because XKr8-mediated exposure of PtdSer occurs during the late stages of apoptosis [42], it is likely that other cellular factors, such as TMEM16F, are involved in PtdSer cell surface exposure and subsequent virion incorporation as a consequence of cell stress during peak viral replication.

We showed that PtdSer exposure during EBOV infection is dependent on calcium, because the use of BAPTA, a calcium chelator, significantly reduced plasma membrane–associated PtdSer (Figure 4). Because XKr8 function is calcium independent [39], it is likely that the contribution of XKr8 to the enrichment virion-associated PtdSer would be limited. Decreased TMEM16F expression resulted in a significant reduction in virion-associated PtdSer, which led in turn to a concomitant significant reduction in viral infectivity (Figure 3). Our results suggest that interfering with TMEM16F function may be of therapeutic value, given that R5421 was shown to reduce viral infectivity (Figure 5). However, because relatively little is known about TMEM16F function across various cell types, further investigation is needed into the cellular processes affected by inhibiting TMEM16F function.

Viral apoptotic mimicry, which is defined by the exposure of PtdSer on the outer leaflet of the viral membrane, has been proposed as a mechanism for virus entry, binding and immune evasion [51]. Our findings suggest that incorporation of PtdSer into the outer leaflet of the viral membrane is a by-product of cell stress, which results from the expression of viral antigens, specifically GP and to a lesser extent VP40. The viral envelope proteins of several viruses, including hepatitis C virus, herpes simplex virus, and HIV, have been shown to increase intracellular Ca^{2+} levels by inducing ER stress [52–54]. This is consistent with our findings that demonstrated transient expression of GP increased cell surface expression of PtdSer via a calcium-dependent mechanism.

A previous study demonstrated that EBOV infection of Vero E6 cells does not lead to translocation of PtdSer, despite

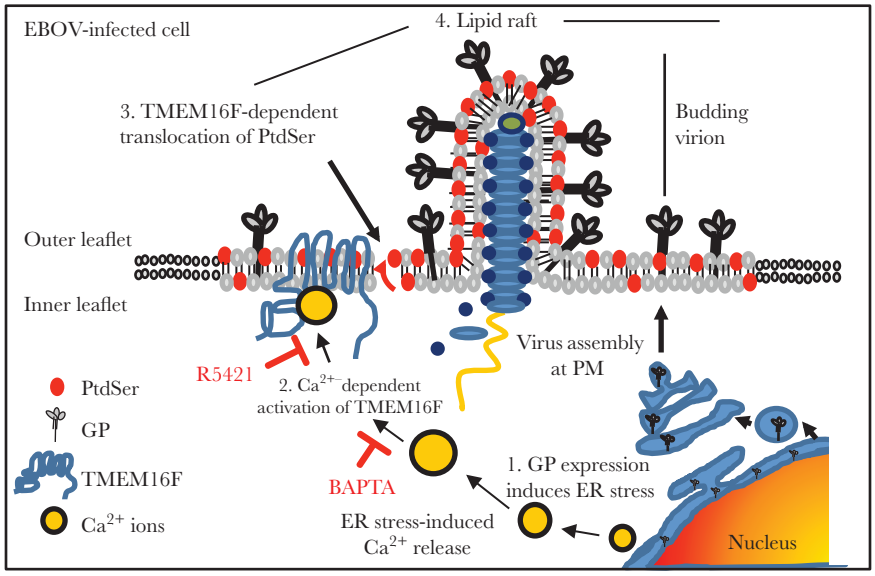

Figure 7. Schematic representation of the role of transmembrane protein 16F (TMEM16F) in the incorporation of phosphatidylserine (PtdSer) into budding virion membranes. Steps are as follows: (1) glycoprotein (GP) expression in the endoplasmic reticulum (ER) activates the ER stress response; (2) increased intracellular calcium (Ca^{2+}) levels trigger TMEM16F activation; (3) TMEM16F mediates translocation of PtdSer from the inner to the outer leaflet of the plasma membrane; (4) PtdSer translocation and Ebola virus (EBOV) budding occur within the lipid raft regions of the plasma membrane. Also shown are the cellular targets inhibited by BAPTA and R5421. Abbreviation: PM, plasma membrane.

detection, albeit at a low level, of cleaved caspase 3 and apoptotic poly(adenosine diphosphate ribose) polymerase 1 [55]. The discrepancy of these data and our data can be related to cell-specific differences; for example, in Vero cells, which are deficient in type I interferon, apoptosis is delayed [56], whereas in our study, interferon-competent Huh7 cells were used. Another study demonstrated that expression of EBOV VP40 protein triggers an increase in host cell cytoplasmic Ca^{2+} levels [57], which indirectly supports our proposed model in which internalization of EBOV particles and/or expression of EBOV proteins triggers release of intracellular Ca^{2+}, leading to activation of TMEM16F and subsequent externalization of PtdSer.

In a larger context regarding the role of PtdSer in apoptotic mimicry, it remains to be determined whether virion-associated PtdSer on its own can modify the immune response, a question that has been indirectly raised elsewhere [39]. It has been suggested that PtdSer in virion envelopes suppresses the inflammatory response by binding to PtdSer receptors, such as the T-cell immunoglobulin and mucin (TIM) family of receptors on phagocytic cells [58]; however, in the context of T cells, both anti–TIM-1 (TIM-1) antibodies and EBOV-associated PtdSer were shown to result in activation and secretion of cytokines [59, 60]. Given that copious amounts of inflammatory mediators are released during EBOV infection, resulting in the onset of the "cytokine storm" phenomenon [61], it is difficult to speculate how virion-associated PtdSer, as well as the extensive amount of PtdSer-enriched apoptotic bodies that exist due to massive, bystander-mediated cell death [7], contribute to immune suppression.

Indeed, several lines of evidence suggest that TIM-1 possesses a dual role in regulation of T-cell–mediated inflammatory responses, which includes both activation and suppression [62]. TIM-1 may play a role as a costimulatory molecule in T-cell activation or transduce inhibitory signals that block effector T-cell function [59, 63, 64]. Hence, the outcome of PtdSer signaling is probably dependent on costimulatory signals. It remains to be determined whether and how blocking PtdSer expression on the outer membrane of virions may have a beneficial outcome beyond reducing viral infectivity, which was observed in the current study.

In conclusion, in the current study, we identified TMEM16F as the calcium-dependent cellular factor responsible for the increased enrichment of PtdSer within the envelope of budding EBOV virions. We showed that decreasing the rate of PtdSer incorporation into virions using shRNAs or pharmacological inhibition of TMEM16F function significantly decreases viral infectivity.

Supplementary Data

Supplementary materials are available at *The Journal of Infectious Diseases* online. Consisting of data provided by the authors to benefit the reader, the posted materials are not copyedited and are the sole responsibility of the authors, so questions or comments should be addressed to the corresponding author.

Notes

Author contributions. P. Y. designed these studies. P. Y. and M. I. performed infections, flow cytometry, and Western blotting experiments. P. Y. and R. I. S. performed confocal microscopy experiments. P. Y. and M. I. performed imaging flow cytometry experiments, including staining of samples and acquisition and analysis of data. P. R. contributed to infection

experiments and sample collection. V. L. P. provided expertise in performing transmission and scanning electron microscopy and interpretation of electron microscopic observations. P. Y. and A. B. initiated the project, and A. B. led the project. P. Y., M. I., R. I. S, P. R., and A. B. composed the manuscript.

Financial support. This work was supported by the National Institutes of Health (grant U19 AI109945-01 to A. B.; Project 2 Molecular Basis for Ebola Virus Immune Paralysis).

Potential conflicts of interest. All authors: No reported conflicts. All authors have submitted the ICMJE Form for Disclosure of Potential Conflicts of Interest. Conflicts that the editors consider relevant to the content of the manuscript have been disclosed.

References

1. Centers for Disease Control and Prevention. 2014 Ebola outbreak in West Africa—case counts. http://www.cdc.gov/vhf/ebola/outbreaks/2014-west-africa/case-counts.html. Accessed May 2018.
2. Feldmann H, Sanchez A, Geisbert TW. Filoviridae: Marburg and Ebola viruses. In: Knipe DM, Howley PM, eds. Fields virology. 6 ed. Philadelphia, PA: Lippincott Williams & Wilkins, **2013**:923–56.
3. Kuhn JH. Filoviruses. 1 ed. Wien New York: Springer, **2008** (Calisher CH, ed.
4. Takada A, Kawaoka Y. The pathogenesis of Ebola hemorrhagic fever. Trends Microbiol **2001**; 9:506–11.
5. Vernet MA, Reynard S, Fizet A, et al. Clinical, virological, and biological parameters associated with outcomes of Ebola virus infection in Macenta, Guinea. JCI Insight **2017**; 2:e88864.
6. Baize S, Leroy EM, Mavoungou E, Fisher-Hoch SP. Apoptosis in fatal Ebola infection: does the virus toll the bell for immune system? Apoptosis **2000**; 5:5–7.
7. Geisbert TW, Hensley LE, Gibb TR, Steele KE, Jaax NK, Jahrling PB. Apoptosis induced in vitro and in vivo during infection by Ebola and Marburg viruses. Lab Invest **2000**; 80:171–86.
8. Reed DS, Hensley LE, Geisbert JB, Jahrling PB, Geisbert TW. Depletion of peripheral blood T lymphocytes and NK cells during the course of Ebola hemorrhagic fever in cynomolgus macaques. Viral Immunol **2004**; 17:390–400.
9. Ebihara H, Rockx B, Marzi A, et al. Host response dynamics following lethal infection of rhesus macaques with *Zaire ebolavirus*. J Infect Dis **2011**; 204 (suppl 3):S991–9.
10. Baize S, Leroy EM, Georges-Courbot MC, et al. Defective humoral responses and extensive intravascular apoptosis are associated with fatal outcome in Ebola virus-infected patients. Nat Med **1999**; 5:423–6.
11. Wauquier N, Becquart P, Padilla C, Baize S, Leroy EM. Human fatal Zaire Ebola virus infection is associated with an aberrant innate immunity and with massive lymphocyte apoptosis. PLoS Negl Trop Dis **2010**; 4.
12. Prescott JB, Marzi A, Safronetz D, Robertson SJ, Feldmann H, Best SM. Immunobiology of Ebola and Lassa virus infections. Nat Rev Immunol **2017**; 17:195–207.
13. Iampietro M, Younan P, Nishida A, et al. Ebola virus glycoprotein directly triggers T lymphocyte death despite of the lack of infection. PLoS Pathog **2017**; 13:e1006397.
14. Rhein BA, Maury WJ. Ebola virus entry into host cells: identifying therapeutic strategies. Curr Clin Microbiol Rep **2015**; 2:115–24.
15. Geisbert TW, Hensley LE, Larsen T, et al. Pathogenesis of Ebola hemorrhagic fever in cynomolgus macaques: evidence that dendritic cells are early and sustained targets of infection. Am J Pathol **2003**; 163:2347–70.
16. Bray M, Geisbert TW. Ebola virus: the role of macrophages and dendritic cells in the pathogenesis of Ebola hemorrhagic fever. Int J Biochem Cell Biol **2005**; 37:1560–6.
17. Mahanty S, Hutchinson K, Agarwal S, McRae M, Rollin PE, Pulendran B. Cutting edge: impairment of dendritic cells and adaptive immunity by Ebola and Lassa viruses. J Immunol **2003**; 170:2797–801.
18. Bosio CM, Aman MJ, Grogan C, et al. Ebola and Marburg viruses replicate in monocyte-derived dendritic cells without inducing the production of cytokines and full maturation. J Infect Dis **2003**; 188:1630–8.
19. Lubaki NM, Younan P, Santos RI, et al. The Ebola interferon inhibiting domains attenuate and dysregulate cell-mediated immune responses. PLoS Pathog **2016**; 12:e1006031.
20. Messaoudi I, Amarasinghe GK, Basler CF. Filovirus pathogenesis and immune evasion: insights from Ebola virus and Marburg virus. Nat Rev Microbiol **2015**; 13:663–76.
21. Lubaki NM, Ilinykh P, Pietzsch C, et al. The lack of maturation of Ebola virus-infected dendritic cells results from the cooperative effect of at least two viral domains. J Virol **2013**; 87:7471–85.
22. Ilinykh PA, Lubaki NM, Widen SG, et al. Different temporal effects of Ebola virus VP35 and VP24 proteins on global gene expression in human dendritic cells. J Virol **2015**; 89:7567–83.
23. Williamson P, Schlegel RA. Back and forth: the regulation and function of transbilayer phospholipid movement in eukaryotic cells. Mol Membr Biol **1994**; 11:199–216.
24. Zwaal RF, Schroit AJ. Pathophysiologic implications of membrane phospholipid asymmetry in blood cells. Blood **1997**; 89:1121–32.
25. Balasubramanian K, Schroit AJ. Aminophospholipid asymmetry: a matter of life and death. Annu Rev Physiol **2003**; 65:701–34.
26. Daleke DL. Regulation of transbilayer plasma membrane phospholipid asymmetry. J Lipid Res **2003**; 44:233–42.
27. Holthuis JC, Levine TP. Lipid traffic: floppy drives and a superhighway. Nat Rev Mol Cell Biol **2005**; 6:209–20.
28. Bhattacharyya S, Zagorska A, Lew ED, et al. Enveloped viruses disable innate immune responses in dendritic cells by direct activation of TAM receptors. Cell Host Microbe **2013**; 14:136–47.
29. Jemielity S, Wang JJ, Chan YK, et al. TIM-family proteins promote infection of multiple enveloped viruses through virion-associated phosphatidylserine. PLoS Pathog **2013**; 9:e1003232.
30. Kondratowicz AS, Lennemann NJ, Sinn PL, et al. T-cell immunoglobulin and mucin domain 1 (TIM-1) is a receptor for *Zaire ebolavirus* and *Lake Victoria marburgvirus*. Proc Natl Acad Sci U S A **2011**; 108:8426–31.
31. Meertens L, Carnec X, Lecoin MP, et al. The TIM and TAM families of phosphatidylserine receptors mediate dengue virus entry. Cell Host Microbe **2012**; 12:544–57.
32. Mercer J, Helenius A. Vaccinia virus uses macropinocytosis and apoptotic mimicry to enter host cells. Science **2008**; 320:531–5.
33. Moller-Tank S, Kondratowicz AS, Davey RA, Rennert PD, Maury W. Role of the phosphatidylserine receptor TIM-1 in enveloped-virus entry. J Virol **2013**; 87:8327–41.
34. Morizono K, Xie Y, Olafsen T, et al. The soluble serum protein Gas6 bridges virion envelope phosphatidylserine to the TAM receptor tyrosine kinase Axl to mediate viral entry. Cell Host Microbe **2011**; 9:286–98.
35. Bavinck JN, Kootte AM, van der Woude FJ, Vandenbroucke JP, Vermeer BJ, Claas FH. HLA-A11-associated resistance to skin cancer in renal-transplant recipients. N Engl J Med **1990**; 323:1350.
36. Leventis PA, Grinstein S. The distribution and function of phosphatidylserine in cellular membranes. Annu Rev Biophys **2010**; 39:407–27.
37. Fadeel B, Xue D. The ins and outs of phospholipid asymmetry in the plasma membrane: roles in health and disease. Crit Rev Biochem Mol Biol **2009**; 44:264–77.
38. Maruri-Avidal L, Weisberg AS, Moss B. Direct formation of vaccinia virus membranes from the endoplasmic reticulum in the absence of the newly characterized L2-interacting protein A30.5. J Virol **2013**; 87:12313–26.
39. Birge RB, Boeltz S, Kumar S, et al. Phosphatidylserine is a global immunosuppressive signal in efferocytosis, infectious disease, and cancer. Cell Death Differ **2016**; 23:962–78.
40. Lorizate M, Sachsenheimer T, Glass B, et al. Comparative lipidomics analysis of HIV-1 particles and their producer cell membrane in different cell lines. Cell Microbiol **2013**; 15:292–304.
41. Bavari S, Bosio CM, Wiegand E, et al. Lipid raft microdomains: a gateway for compartmentalized trafficking of Ebola and Marburg viruses. J Exp Med **2002**; 195:593–602.
42. Suzuki J, Denning DP, Imanishi E, Horvitz HR, Nagata S. Xk-related protein 8 and CED-8 promote phosphatidylserine exposure in apoptotic cells. Science **2013**; 341:403–6.
43. Nanbo A, Maruyama J, Imai M, et al. Ebola virus requires a host scramblase for externalization of phosphatidylserine on the surface of viral particles. PLoS Pathog **2018**; 14:e1006848.
44. Suzuki J, Umeda M, Sims PJ, Nagata S. Calcium-dependent phospholipid scrambling by TMEM16F. Nature **2010**; 468:834–8.
45. Towner JS, Paragas J, Dover JE, et al. Generation of eGFP expressing recombinant *Zaire ebolavirus* for analysis of early pathogenesis events and high-throughput antiviral drug screening. Virology **2005**; 332:20–7.
46. Lubaki NM, Ilinykh P, Pietzsch C, et al. The lack of maturation of Ebola virus-infected dendritic cells results from the cooperative effect of at least two viral domains. J Virol **2013**; 87:7471–85.
47. Meyer M, Garron T, Lubaki NM, et al. Aerosolized Ebola vaccine protects primates and elicits lung-resident T cell responses. J Clin Invest **2015**; 125:3241–55.
48. Willms E, Johansson HJ, Mäger I, et al. Cells release subpopulations of exosomes with distinct molecular and biological properties. Sci Rep **2016**; 6:22519.

49. Geisbert TW, Jahrling PB. Differentiation of filoviruses by electron microscopy. Virus Res **1995**; 39:129–50.
50. Gonzalez LJ, Gibbons E, Bailey RW, et al. The influence of membrane physical properties on microvesicle release in human erythrocytes. PMC Biophys **2009**; 2:7.
51. Amara A, Mercer J. Viral apoptotic mimicry. Nat Rev Microbiol **2015**; 13:461–9.
52. Pavio N, Romano PR, Graczyk TM, Feinstone SM, Taylor DR. Protein synthesis and endoplasmic reticulum stress can be modulated by the hepatitis C virus envelope protein E2 through the eukaryotic initiation factor 2alpha kinase PERK. J Virol **2003**; 77:3578–85.
53. Mulvey M, Arias C, Mohr I. Maintenance of endoplasmic reticulum (ER) homeostasis in herpes simplex virus type 1-infected cells through the association of a viral glycoprotein with PERK, a cellular ER stress sensor. J Virol **2007**; 81:3377–90.
54. Shah A, Vaidya NK, Bhat HK, Kumar A. HIV-1 gp120 induces type-1 programmed cell death through ER stress employing IRE1α, JNK and AP-1 pathway. Sci Rep **2016**; 6:18929.
55. Olejnik J, Alonso J, Schmidt KM, et al. Ebola virus does not block apoptotic signaling pathways. J Virol **2013**; 87:5384–96.
56. Zhirnov OP, Konakova TE, Wolff T, Klenk HD. NS1 protein of influenza A virus down-regulates apoptosis. J Virol **2002**; 76:1617–25.
57. Han Z, Madara JJ, Herbert A, et al. Calcium regulation of hemorrhagic fever virus budding: mechanistic implications for host-oriented therapeutic intervention. PLoS Pathog **2015**; 11:e1005220.
58. Moller-Tank S, Maury W. Phosphatidylserine receptors: enhancers of enveloped virus entry and infection. Virology **2014**; 468-470:565–80.
59. Umetsu SE, Lee WL, McIntire JJ, et al. TIM-1 induces T cell activation and inhibits the development of peripheral tolerance. Nat Immunol **2005**; 6:447–54.
60. Younan P, Iampietro M, Nishida A, et al. Ebola virus binding to Tim-1 on T lymphocytes induces a cytokine storm. MBio **2017**; 8.
61. Marcinkiewicz J, Bryniarski K, Nazimek K. Ebola haemorrhagic fever virus: pathogenesis, immune responses, potential prevention. Folia Med Cracov **2014**; 54:39–48.
62. Baghdadi M, Jinushi M. The impact of the TIM gene family on tumor immunity and immunosuppression. Cell Mol Immunol **2014**; 11:41–8.
63. de Souza AJ, Oriss TB, O'malley KJ, Ray A, Kane LP. T cell Ig and mucin 1 (TIM-1) is expressed on in vivo-activated T cells and provides a costimulatory signal for T cell activation. Proc Natl Acad Sci USA **2005**; 102:17113–8.
64. Encinas JA, Janssen EM, Weiner DB, et al. Anti-T-cell Ig and mucin domain-containing protein 1 antibody decreases TH2 airway inflammation in a mouse model of asthma. J Allergy Clin Immunol **2005**; 116:1343–9.